Micro-Transfer-Printing of Al₂O₃-Capped Short-Wave-Infrared PbS Quantum Dot Photoconductors

Nayyera Mahmoud,*,†,‡,¶ Willem Walravens,‡,¶ Jakob Kuhs,§ Christophe Detavernier,§ Zeger Hens,‡,¶ and Gunther Roelkens†,‡

†Photonics Research Group, Ghent University-imec, Technologiepark-Zwijnaarde 15, B-9052 Zwijnaarde, Belgium
‡Center for Nano and Biophotonics, Ghent University-imec, Technologiepark-Zwijnaarde 15, B-9052 Zwijnaarde, Belgium
¶Physics and Chemistry of Nanostructures (PCN), Ghent University, Krijgslaan 281-S3, Ghent 9000, Belgium
§Conformal Coating of Nanomaterials (CoCooN), Ghent University, Krijgslaan 281-S1, Ghent 9000, Belgium

Ⓢ Supporting Information

ABSTRACT: Quantum dots (QDs) have attracted considerable attention in the development of various optoelectronic applications. The scalable heterogeneous integration of high quality, yet stable QD films is required for low-cost devices based on these materials. Here, we demonstrate the transfer printing of microscale patterns of Al₂O₃-capped PbS QD films to realize large-scale integrated photodetector arrays with a first excitonic absorption peak at 2.1 μm wavelength. The process provides a facile approach to selectively pick-and-print QD assemblies on device structures with high precision. Transfer-printed photoconductor devices were realized and characterized at low bias voltage and optical power. Under 10 nW surface normal illumination at 2.1 μm wavelength, the responsivity of our devices obtained at 1 V bias reached a maximum value of 25 A/W and 85 A/W for PbS QD films of 88 and 140 nm thick, respectively. Our approach suggests new routes toward scalable and cost-effective integration of multiple high-quality QD stacks on electronic and optoelectronic circuits.

KEYWORDS: short-wave infrared, colloidal quantum dots, ALD, micro-transfer-printing, photoconductors
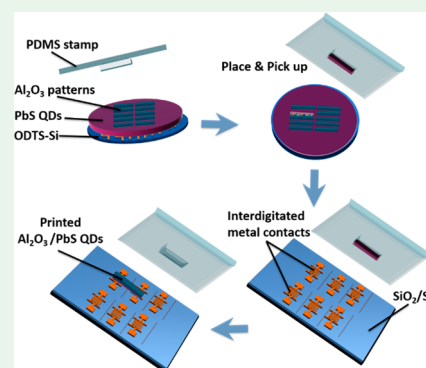
1. INTRODUCTION

The short-wave infrared (SWIR, 0.9−3 μm) spectral range enables a wide range of applications, including hyperspectral imaging, on-chip-biosensing based on spectral signatures derived from molecular vibrations, night time surveillance, and optical communications.[1−5] Detector arrays based on III−V semiconductors, such as InGaAs, are currently driving these applications because of their high quantum efficiency and low dark current at room temperature.[6] Unfortunately, the high material and fabrication cost per unit area prohibit the penetration of the technology into consumer applications. Moreover, monolithic integration on low-cost Si electronics is difficult because of the lattice mismatch between IR materials such as InGaAs and silicon, requiring a hybrid integration through flip-chip bonding.[7] Ideally, a good photodetector technology has to address the challenge of mass fabrication by relying on a relatively cheap material with high photoresponse that can easily be integrated on commercial silicon read-out integrated circuits.

Colloidal quantum dots (CQDs) are promising, novel materials for photodetection due to their unique optical properties. The broad addressable spectrum with a sharp and tunable absorption onset based on size control, the high quantum efficiency and photostability make CQDs a suitable alternative to epitaxially grown semiconductors.[8] Moreover, colloidal synthesis is a low-cost fabrication approach that enables the QD size, shape, and surface chemistry to be tuned, thereby optimizing the optoelectronic properties of the QDs for the envisioned application.[9,10]

Infrared colloidal lead chalcogenides (PbX) nanocrystals (such as PbS CQDs) are the most extensively used and commercially available colloidal material for the SWIR region. Various techniques are developed for the integration of CQDs as thin films in electronic and optoelectronic devices. This is conventionally done by techniques that use CQD dispersions, such as drop casting,[11] spin coating,[12] dip coating,[13] Langmuir−Blodgett deposition,[14] and doctor blading.[15] Generally, such methods enable low-cost, low-temperature, and large area formation of QD-based micro- and nanoscale devices.

Despite the simplicity of these techniques, to realize functional QD-based devices, postprocessing steps to pattern integrated QD films are still required. Several patterning approaches are reported, each with its advantages and limitations. Microscale QD patterns were realized using photolithography either through lift-off[16] or wet etching.[17]
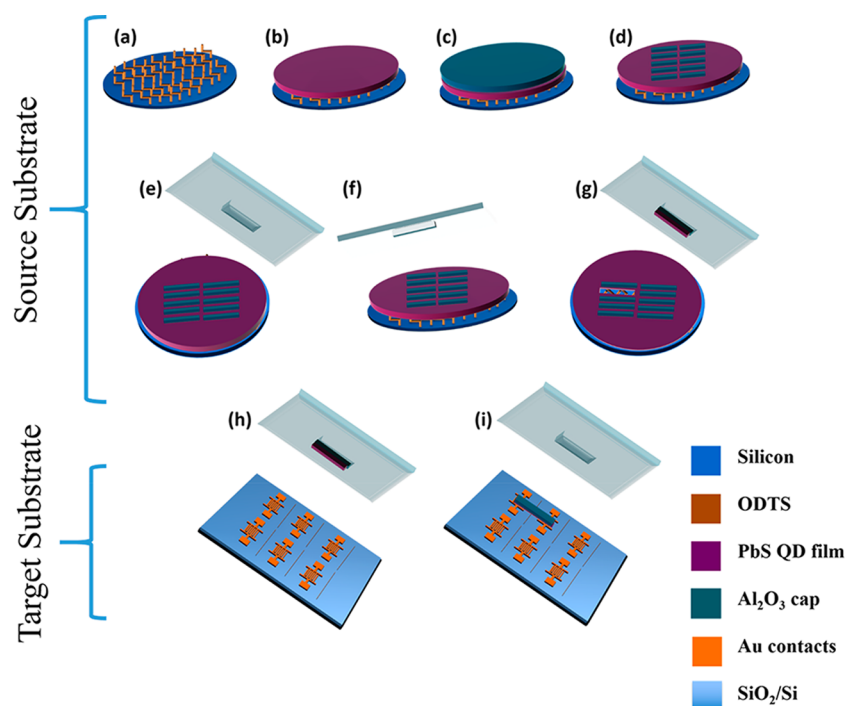
Figure 1. Schematic illustration of the transfer printing process flow. (a–d) Source substrate preparation, which starts with surface modification by ODTS-SAM, QD film spin coating with layer-by-layer ligand exchange, and finally deposition and patterning of ALD-Al₂O₃. (e–i) Transfer printing of Al₂O₃/PbS patches on multiple interdigitated electrodes realized on an oxidized silicon wafer resulting in the formation of a series of photoconductors per single transfer printing operation.

High-resolution nanoscale patterning of QD films was realized by electron beam lithography.[18] These methods are limited in usable QD film thickness and surface chemistry and suffer from cross contamination by organic photoresists and chemicals used during etching. Such challenges drive the exploration of new techniques for the scalable integration of uniform, well-defined QD films on a substrate, together with other materials.

Another significant challenge is the deterioration of performance of QD-based devices because of irreversible changes of the QDs surface termination, causing a drop in, for example, the photoluminescence quantum yield. This is attributed to the shift of the QD Fermi energy upon oxidation by direct exposure to ambient air. Therefore, to extend the photostability lifetime of QDs, encapsulation strategies are required, where organic[19] and inorganic[20] coatings are used. An interesting approach for QD encapsulation is using atomic layer deposition (ALD), which provides a self-limiting, conformal growth process for surface coatings with nanometer thick films of metal oxides such as Al₂O₃, HfO₂, TiO₂, or ZnO.[21] Thermal ALD grown Al₂O₃ on QD films was reported to successfully provide an efficient encapsulation layer for the protection of QD-based device stacks against oxidation.[22−25]

In this work, we present the first realization of air-stable SWIR PbS photoconductor arrays through micro-transfer-printing. Micron-sized Al₂O₃-capped PbS QD (Al₂O₃/PbS QD) patterns are selectively transferred onto arrays of planar interdigitated (Ti/Au) electrodes on a thermally oxidized silicon substrate, mimicking an underlying electronic read-out circuit, using a structured poly-dimethyl-siloxane (PDMS) stamp. We demonstrate a protocol for a facile solvent-free transfer of multiple high-quality Al₂O₃-capped QD patches to the target substrate per single print. The transfer is done from a densely populated QD/Si source substrate, allowing maximum

usage of the deposited QD films to print on multiple substrates. The to-be-transferred QD film area is defined by a facile and fast patterning of the Al₂O₃ using photolithography followed by wet etch. Only patterning the Al₂O₃ is sufficient to peel-off thick QD films underneath the Al₂O₃ during the transfer printing process. This introduces an efficient way for wafer-scale integration of QD patches/devices on either electronic or photonic circuits, or any other substrate. The fabrication of the source substrate is entirely done in glovebox conditions. The bare QD source substrates are then sealed and transferred in a vacuum bag to the ALD machine for Al₂O₃ deposition to ensure no air exposure until the Al₂O₃ capping is realized. A detailed transfer printing process flow of Al₂O₃/PbS QD films from the source substrate to the target substrate is reported. Finally, current–voltage measurements in dark and under low optical intensities at 2.1 μm wavelength are carried out to evaluate the performance of the realized devices.

2. RESULTS AND DISCUSSION

2.1. Transfer Printing Process Flow. The transfer printing is realized by a commercial micro-transfer-printer (X-Celeprint, model μTP-100). The printing process involves using a patterned PDMS stamp installed on a glass holder to pick up the material from the source substrate placed onto the source chuck. Then the stamp moves to the target chuck and prints with a submicrometer accuracy on a predefined position on the target substrate. After completion, the stamp moves and presses down on a cleaning pad to remove residual print material (if necessary).[26] In our presented work, arrays of Al₂O₃/PbS QD patches (realized on the source substrate) are printed on prefabricated interdigitated contact electrodes on the target substrate. In this process, a 100 μm × 800 μm patterned PDMS post is used to pick up and print the desired
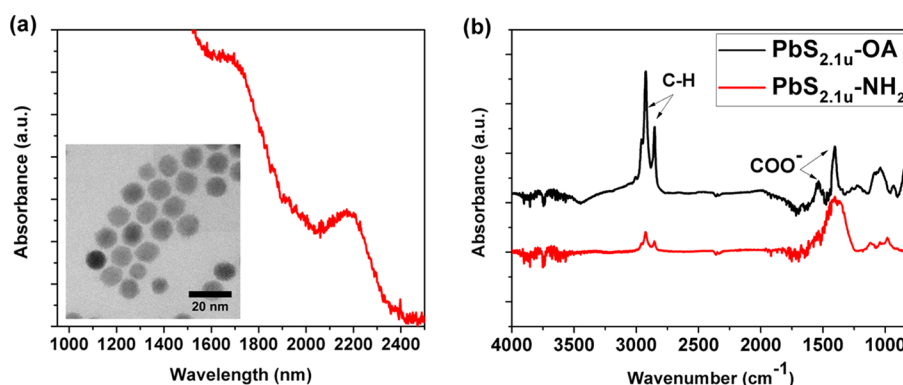
Figure 2. (a) Absorption spectrum of OA-terminated colloidal PbS QDs. (b) FTIR spectra of oleate-capped PbS QD film (black) and butylamine-capped PbS QDs (red). (inset of panel a) Transmission electron micrograph of oleate-capped PbS QDs.

material. Picking and printing is realized by controlling the adhesion of the QD patch to the stamp.[27,28] The position of the QD patches on the source substrate as well as the position of the devices on the target wafer are predefined to allow a fully automated transfer printing operation. The alignment of the stamp with source and target substrate is monitored by a camera mounted on top of the transparent stamp and stamp holder. A schematic illustration of the transfer-printing process flow is shown in Figure 1. In addition, a cross-section view is presented in Figure S1.

Preparation of source substrates starts with using PbS QDs (11.8 nm) synthesized by adapting the method introduced by Jonathan S. Owen and his co-workers.[29] According to the absorbance spectrum shown in Figure 2a, the obtained PbS QDs exhibit a first excitonic transition at λ = 2.1 μm. The quality and particle size distribution was confirmed by TEM shown in Figure 2a, inset.

Silicon (Si) substrates are first modified with self-assembled octadecyltrichlorosilane (ODTS) monolayers to facilitate delamination during the transfer printing process. The interaction that occurs between the silane precursor and the silanol group presented on the Si surface result in the formation of highly ordered, immobilized alkyl chains of organic silane. Piranha treatment was performed before the reaction to introduce an oxide layer on the Si (100) surface, where the terminated −OH groups served as active sites to link the alkyl ODTS. This results in a heterogeneous structure with densely packed alkyl chains, almost arranged perpendicular to the Si surface.[30] Such functional groups substantially diminish the surface energy without introducing surface roughness (only ∼0.2 nm) and shows a good adherence to the primary QD layer, resulting in a uniform QD film.[31]

CQD film deposition is made by means of a layer-by-layer spin coating on the ODTS-Si substrates. For each coated layer, the native oleic acid ligands were removed upon exposure to a (1 M) n-butylamine in methanol (MeOH) solution. These deposition cycles were repeated until the desired film thickness was reached. The ligand exchange was confirmed using Fourier transform infrared spectroscopy (FTIR). Figure 2b illustrates the FTIR spectra of a QD film before and after exposure to the n-butylamine solution. The signatures of the COO$^-$ and C−H vibrations in the range of 1300−1500 and 2800−3000 cm^{-1}, respectively, indicate the presence of oleate ligands at the QD surface.[32,33] The substantial reduction of the intensity of these features confirms the ligands removal. The resulting dry QD film is then capped through a thermal ALD deposition of

Al$_2$O$_3$ to form a 70 nm thick layer.[34] Finally, a dense array of Al$_2$O$_3$ patterns on top of the PbS QD films is realized through photolithography and subsequent wet etching. It is worth noting that during the transfer-printing process, the capped QD patches were still covered by this photoresist layer (∼3.5 μm thick) to prevent the brittle patches from being damaged during printing on the target substrate. For target substrates, planarized arrays of interdigitated Ti/Au contacts were defined through optical lithography, e-beam metal deposition, and lift-off on a thermally oxidized silicon wafer. Before metal deposition, the SiO$_2$ is partially etched through reactive ion etching (RIE) with the same pattern as the interdigitated finger electrodes such that after metal pattern definition planar substrates are achieved with a surface topography of 5 nm.

The strong interactions between the QD surface and the Al$_2$O$_3$ film compared to the weak binding energy at the ODTS-Si surface allow excellent kinetic control of the QD patterning/pickup from the source without the need to exert a high stamp pressure or a slow retraction of the stamp to peel-off the pattern. The Al$_2$O$_3$/PbS QDs stripes were peeled off at a peeling velocity 70 mm·s^{-1}, resulting in a uniform film. Previous reported procedures[35−37] on QD transfer printing showed pick-up of bare QD films with a thickness of 30 nm. However, our presented work allows effective dry patterning and transfer of relatively thick QD films along with the Al$_2$O$_3$ capping layer. For comparison, transfer printing of a bare PbS QD stack (140 nm) without the Al$_2$O$_3$ capping layer results in a significant nonuniformity with several cracks and voids that will affect the performance of the devices made out of these films, as shown in Figure S2. A comparison between the transfer printing of bare QD and Al$_2$O$_3$/PbS QD films is shown in Table S1. It is yet interesting to do a further study on thicker samples to validate what the maximum thickness of transfer-printable QD films is. The presence of the Al$_2$O$_3$ cap layer enhances the transfer printing process by forming an "exoskeleton" for the QD film and providing a fast and high-quality pickup. This leads to the conclusion that the Al$_2$O$_3$ layer not only protects the QDs against oxidation, but also facilitates QD film patterning and improves the pick-up yield and printing throughput.

Figure 3a shows an optical image of a well-defined vacant area on the source substrate after pick-up of an Al$_2$O$_3$/QD patch, while the bare QD film still is present around the peeled area. Figure 3b shows an SEM image after printing of this patch on three-in-a-row interdigitated Ti/Au electrodes (after removal of the protective photoresist on top of the quantum
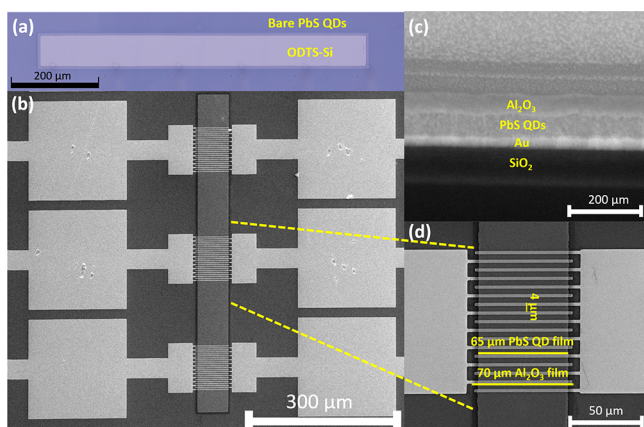
Figure 3. (a) Optical image of the source substrate after pattern pick-up, (b) transfer-printed Al$_2$O$_3$/PbS QD film, (c) cross section on a pair of interdigitated Au contacts, and (d) zoom-in on a single photoconductor.

dot patch using acetone). As discussed above, the Ti/Au electrodes were planarized to enable a smooth transfer of the QD material. A cross section (Figure 3c) of the transfer-printed patterns validate a good contact with the Au electrodes. Figure 3d shows a zoom-in on a single photoconductor device.

The patches were printed by peeling the stamp at a relatively slow peeling rate to allow a high-quality release (0.2 mm/s). Figure 4 shows an optical microscope image of multiple Al$_2$O$_3$/
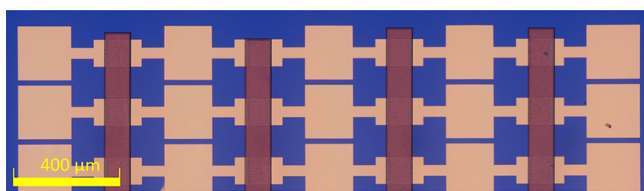
Figure 4. Optical image of multiple arrays of printed Al$_2$O$_3$/PbS QD patches on interdigitated electrodes.

PbS QD patches of different lengths and widths printed with high yield. This demonstrates the excellent scalability of printing high-quality Al$_2$O$_3$-capped QDs with high precision ($\pm$ 1.5 μm 3σ alignment accuracy). The impact of the QD film thickness on the micro-transfer-printing yield was evaluated by transfer printing QD films of 88, 110, and 140 nm thickness, all capped with 70 nm Al$_2$O$_3$. In all three cases, arrays of QD films

were 100% successfully defined, picked-up, and printed on target devices with high precision.

2.2. Al$_2$O$_3$/PbS QD Photoconductor Characterization.

Two different photoconductor structures with QD film thickness of 88 and 140 nm were characterized. The fabricated devices are 80 × 80 μm^2 in area, with interdigitated metal fingers of 80 μm long, 2 μm wide, and on a pitch of 4 μm. Each device is provided with two contact pads of 100 × 100 μm^2. Figure 5a displays typical current−voltage curves of a printed Al$_2$O$_3$/PbS QD device with a 140 nm QD film thickness in the dark and under illumination at 2.1 μm wavelength. The linear behavior of the dark/photocurrent indicates excellent ohmic contacts, which reflects the high quality of the printed Al$_2$O$_3$/PbS patches. The dark resistance (R_d) is about 65 kΩ, which drops by more than 50% (30 kΩ) under 140 μW optical illumination. The responsivity (R) as a function of applied voltage is calculated from the net photocurrent, based on the eq 1

$$R = \frac{I_{\text{light}} - I_{\text{dark}}}{P_{\text{in}}} \qquad (1)$$

where I_{light} is the total current under illumination, I_{dark} is the dark current, and P_{in} is the optical input power. The responsivity shows a linear behavior with the applied bias voltage, as shown in Figure 5b.

The detector responsivity was investigated at low bias voltage (1 V) to evaluate the potential integration to CMOS read-out circuits. Figure 6a and 6b shows the responsivity of the two detectors as a function of incident input power. The responsivity shows a strong power dependence reaching a maximum value of about 85 and 25 A/W at 10 nW illumination for 88 and 140 nm thick PbS QD devices, respectively. Upon illumination, a primary photocurrent arises by photon absorption causing the creation electron−hole pairs. The large responsivity is attributed to the characteristic high gain of photoconductors because of the long lifetime of the photogenerated carriers with respect to transit time. At low illumination levels, all photogenerated carriers are captured by the QD deep surface traps, resulting in a longer lifetime and therefore a higher responsivity. At higher illumination levels, the photogenerated carrier density is expected to exceed the capacity of deep trap states, thereby diminishing the photoresponse. The measured responsivity is in line with previously reported PbS photoconductors.[34,38] Figures S3 and S4 show an evaluation of the responsivity and dark current over 10 transfer printed Al$_2$O$_3$/PbS QD photoconductors of PbS film thickness
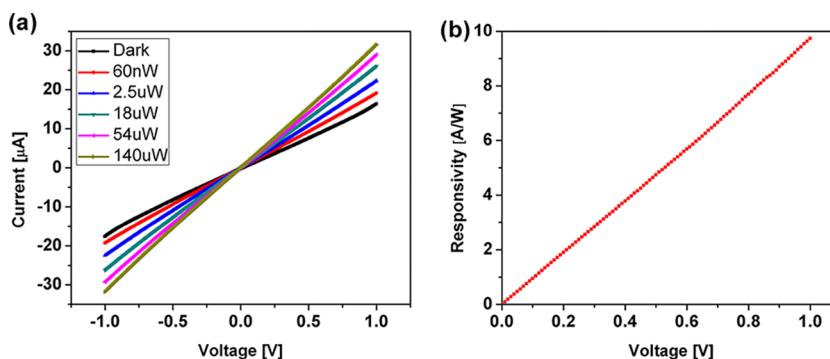
Figure 5. (a) Current−voltage characteristics for surface illumination at 2.1 μm wavelength. (b) Responsivity versus bias voltage for 1 μW optical input power
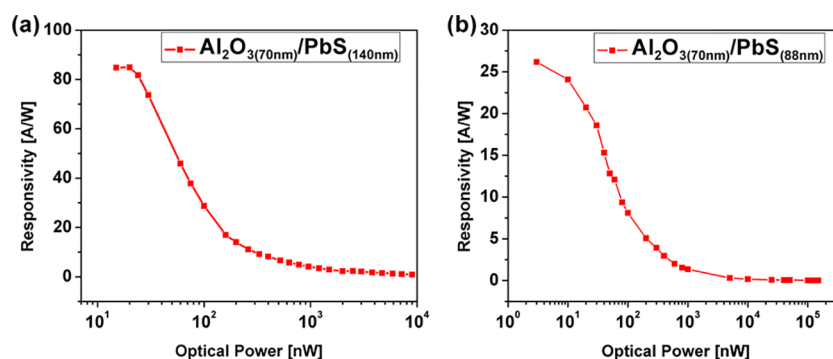
Figure 6. (a) Responsivity versus optical power of Al_2O_3 (70 nm)/PbS(140 nm) and (b) Al_2O_3 (70 nm)/PbS (88 nm) photoconductors, respectively. Responsivity is measured at 1 V applied bias for optical input powers ranging from 10 nW to 140 μW.

88 nm and 10 transfer printed devices of 140 nm PbS film thickness, respectively.

Covering the QD films with Al_2O_3 during transfer printing proved to be effective to avoid degradation with time at ambient conditions. The capped devices showed no degradation over 16 days, at least. Longer lifetime tests are currently ongoing. Nevertheless, the relatively long stability of the devices leaves sufficient time for capping the sides of the printed QD patches on the target wafer.

The wavelength-dependent photoresponse of the Al_2O_3 (70 nm)/PbS(140 nm) photoconductors is shown in Figure 7 (1 μW illumination and 1 V bias). The responsivity spectrum reflects the absorption spectrum of the PbS QDs shown in Figure 2a.
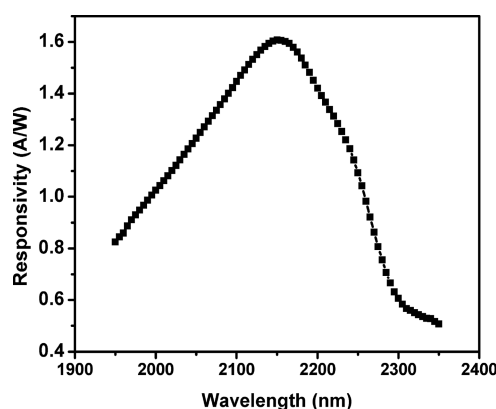
Figure 7. Spectral photoresponse of the Al_2O_3 (70 nm)/PbS (140 nm) photoconductors measured in the spectral range from 1950 to 2350 nm at 1 μW optical illumination and 1 V bias.

The time response of the printed devices was also investigated by modulating the laser illumination and biasing the device at 1 V. The measurement setup scheme and typical time response are shown in Figure 8. Upon illumination the photocurrent rises first quickly and then increases at a slower rate until reaching steady state. A similar effect can be seen when switching off. This is attributed to the existence of both deep (long-lived) trap states and shallow (short-lived) trap states. The rise time τ_r is 2.25s while the fall time τ_f is 5.6 s. This is expected behavior for photoconductors, which exhibit a high responsivity but slow response time especially at low optical illumination levels.[34,38]

3. CONCLUSION

We report the micro-transfer-printing of Al_2O_3/PbS photoconductors on interdigitated electrode structures. Our approach allows the efficient integration of well-defined, air-stable and high-quality QD films. The Al_2O_3 cap plays an important role in QD pattern definition, facile transfer-printing, and protection from oxidation. The pick-up and printing were optimized to reach close to 100% yield. Photoconductors developed using this approach exhibit high responsivity at 2.1 μm with maximum values of 25 and 85 A/W for QD films of thickness 88 and 140 nm, respectively, at 1 V bias. This transfer printing approach enables the intimate integration of QD films/photoconductors with different cutoff wavelengths, enabling advanced, low-cost devices, such as SWIR hyperspectral imagers.

4. EXPERIMENTAL SECTION

4.1. Synthesis of Colloidal PbS QDs. In a three-neck flask, 0.939 g of Pb-oleate and 10 mL of *n*-dodecane were mixed and heated to 150 °C. Into this solution was injected 1.25 mL of a 0.16 M solution of *N*-hexyl-*N*′-dodecylthiourea in diglyme. Five minutes later, a second injection of 0.75 mL of a 0.8 M solution of *N*-hexyl-*N*′-dodecylthiourea in diglyme was injected. After a total reaction time of 20 min, the reaction was quenched and the QDs precipitated by injecting 10 mL of methyl acetate. After separation by centrifugation, the resulting black pellet was purified further by washing 4 additional times with toluene and methyl acetate as solvent and antisolvent, respectively. Synthesis of *N*-hexyl-*N*′-dodecylthiourea was done by a stirring solution of 6.47 g of dodecylamine (34.9 mmol, 1 equiv) in 20 mL of toluene, and 5.0 g of hexyl isothiocyanate (34.9 mmol, 1 equiv) was added. After the mixture was cooled to room temperature, the white precipitate was dried in vacuum for 24 h.

4.2. Source Substrate Preparation. *4.2.1. Silicon (Si) Cleaning.* Si substrates were cleaned by first rinsing with acetone, isopropyl alcohol (IPA), and deionized (DI) water, followed by a 30 min O_2 plasma treatment. The samples were then treated by 10% HF solution for 5 min to remove the native silicon oxide. Next, a piranha treatment (H_2SO_4:H_2O_2 of ratio 2:1) was applied at 80 °C for 20 min to facilitate the silanization step. Finally, the substrates were rinsed with water, dried with N_2, and stored in a glovebox for further use.

4.2.2. Synthesis of ODTS-Si. A self-assembled monolayer (SAM) of silane was covalently bonded to Si through a chemical reaction of the hydrogen-terminated Si surface with a 10 mM solution of octadecyltrichlorosilane in anhydrous hexane for 2 h under N_2 condition. The substrates were then baked for 20 min at 120 °C to ensure covalent cross-linking on the entire surface. Eventually, the substrates were cleaned by ultrasonication with chloroform and DI water to eliminate extra-unbonded alkylsilanes.

4.2.3. PbS QDs Deposition. Films were completely prepared under N_2 in a glovebox. The film deposition was done through a layer-by-
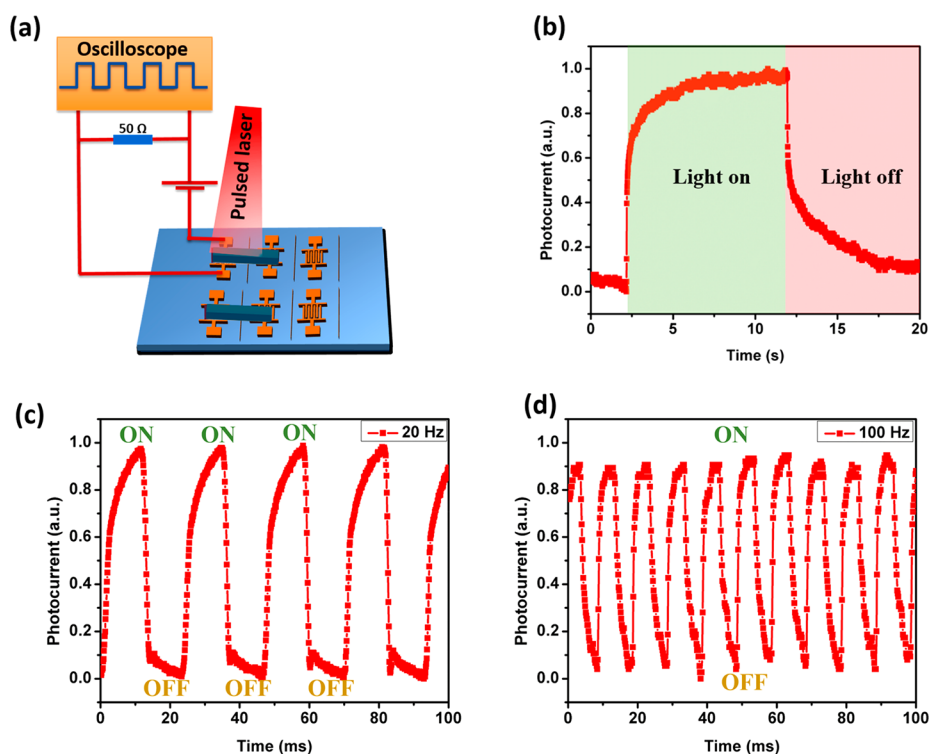
Figure 8. Time response of the Al_2O_3 (70 nm)/PbS (140 nm) devices to periodic on/off laser modulation at 1 V bias. (a) Schematic illustration of the measurement setup. (b) time response of (b) single on/off transition, (c) at 20 Hz, and (d) at 100 Hz modulation frequency.

layer spin coating of a solution of 20 mg/mL OA-PbS QDs (in heptane) at 2000 rpm for 15 s. OA-PbS QDs were then decapped by dipping the substrate for 1 min in 1 M *n*-butylamine in methanol solution, followed by rinsing in pure methanol to reveal the surface of the nanoparticles by removing extra *n*-butylamine. The resulting layer was dried by N_2 before the deposition was repeated to obtain the desired QD film thickness. A thickness of around 88 and 140 nm was achieved by 5 and 8 coating cycles, respectively.

4.2.4. Al_2O_3 ALD Process. A thermal ALD process was carried out in a home-built pump type ALD reactor, with a base pressure of 2×10^{-6} mbar, using trimethylaluminum (TMA) and H_2O as precursors. The deposition temperature was 100 °C. The samples were exposed to 5 s of TMA and 5 s of water vapor at a pressure 5×10^4 Pa. 1000 ALD cycles resulted in a typical 70 nm thick Al_2O_3 film.

4.2.5. Micropatterning of Al_2O_3. Standard photolithography was done, where AZ5214E positive resist was spin coated on the samples and baked at 120 °C for 3 min. The substrates were exposed through a contact photomask using a SUSS MA6 mask aligner and then were developed in AZ400 developer. Subsequently, a diluted KOH solution of pH 12 was used to etch the exposed parts of the Al_2O_3 layer.

4.3. Target Substrate Preparation. A series of patterned metal contacts were fabricated on a thermally oxidized silicon wafer. The oxide thickness was 300 nm. Planarized interdigitated Ti/Au contacts were fabricated by a combination of RIE (Advanced Vacuum Vision 310) dry etching of the SiO_2, e-beam Ti/Au metal evaporation in the formed trenches and subsequent lift-off. The metal fingers are 80 μm long and 2 μm wide and have a pitch of 4 μm. Each device is provided with two contact pads of area 100×100 μm^2.

4.4. Transfer Printing. Transfer printing was carried out using an X-Celeprint micro-TP100 lab-scale printer. A patterned viscoelastic PDMS stamp, with a post of 100 μm $\times$ 800 μm, was laminated against the source substrate with a slight overdrive, then quickly peeled back to lift the as-fabricated Al_2O_3 pattern along with the underlying PbS QD film, thereby transferring the structure to the PDMS stamp. The patterns were covered with resist during the transfer printing operation to prevent cracking of the film by the pressure applied during printing. The pick-up velocity applied was optimized at 70 mm·s^{-1} to reach a pick-up yield of 100%. Printing the patterns was accomplished by laminating the stamp against the target substrate and peeling back at a slow rate (0.2 mm·s^{-1}) for a clean, crack-free release. Finally, the substrates were washed in acetone and IPA to remove photoresist.

4.5. Characterization of Materials and Devices. UV−vis−NIR spectrum of the synthesized colloidal PbS QDs was obtained using a PerkinElmer Lambda 950 spectrophotometer equipped with deuterium and halogen lamps. The particles morphology was evaluated using JEOL 2100 Transmission electron microscopy (TEM). Ligand removal after QD film deposition on ODTS-Si substrates was assessed by Fourier Transform infrared spectroscopy (FTIR), using a Vertex 70v from Bruker attached with a mercury cadmium telluride (MCT) detector cooled by liquid nitrogen. The thickness of ALD grown Al_2O_3 on QD films was monitored by ellipsometry (Woollam M-2000 system) and X-ray reflectivity (XRR) (Bruker D8 Discover, Cu Kα source) measurement. The final devices topography, after transfer printing, were characterized through scanning electron microscopy on a FEI Nova 600 Nanolab Dual-Beam FIB SEM (FEI, Cambridge, UK).

4.6. Optoelectronic Characterization of Devices. Current−voltage measurements were taken in ambient conditions, using a Keithley measure unit. Photocurrent under different illumination levels was measured by surface illumination of the photoconductors with a standard single mode fiber (SMF-28)-coupled laser at 2.1 μm wavelength. The bias was swept between −1 and +1 V with a step of 10 mV. Spectral response was measured by sweeping the laser wavelength, which was monitored by an optical spectrum analyzer (OSA, Yokogawa AQ6375). The time-response measurement was taken by modulating the light using a Thorlabs optical chopper (20 Hz to 1 kHz), where the signal is detected through a 50 Ω load resistor by using an oscilloscope (Keysight DSOX2022A).

■ ASSOCIATED CONTENT

ⓢ Supporting Information

The Supporting Information is available free of charge on the ACS Publications website at DOI: 10.1021/acsanm.8b01915.

Cross-section view of the transfer printing process approach; optical image of transfer printed bare PbS QD stack (140 nm) on silicon substrate without Al_2O_3 cap layer; table showing a comparison between the transfer printing of bare QD and Al_2O_3/PbS QD films; and dark current evaluation across multiple printed devices (PDF)

■ AUTHOR INFORMATION

Corresponding Author

*E-mail: nayyera.mahmoud@ugent.be.

ORCID ●

Nayyera Mahmoud: 0000-0001-5524-7770

Willem Walravens: 0000-0002-9980-6367

Jakob Kuhs: 0000-0003-4723-0578

Christophe Detavernier: 0000-0001-7653-0858

Zeger Hens: 0000-0002-7041-3375

Gunther Roelkens: 0000-0002-4667-5092

Notes

The authors declare no competing financial interest.

■ REFERENCES

(1) Kagan, C. R.; Lifshitz, E.; Sargent, E. H.; Talapin, D. V. Building Devices from Colloidal Quantum Dots. *Science* **2016**, *353*, aac5523.

(2) García de Arquer, F. P.; Armin, A.; Meredith, P.; Sargent, E. H. Solution-Processed Semiconductors for Next-Generation Photodetectors. *Nat. Rev. Mater.* **2017**, *2*, 16100.

(3) Bruns, O. T.; Bischof, T. S.; Harris, D. K.; Franke, D.; Shi, Y.; Riedemann, L.; Bartelt, A.; Jaworski, F. B.; Carr, J. A.; Rowlands, C. J.; Wilson, M. W. B.; Chen, O.; Wei, H.; Hwang, G. W.; Montana, D. M.; Coropceanu, I.; Achorn, O. B.; Kloepper, J.; Heeren, J.; So, P. T. C.; Fukumura, D.; Jensen, K. F.; Jain, R. K.; Bawendi, M. G. Next-Generation In Vivo Optical Imaging with Short-Wave Infrared Quantum Dots. *Nat. Biomed. Eng.* **2017**, *1*, 0056.

(4) Supran, G. J.; Song, K. W.; Hwang, G. W.; Correa, R. E.; Scherer, J.; Dauler, E. A.; Shirasaki, Y.; Bawendi, M. G.; Bulović, V. High-Performance Shortwave-Infrared Light-Emitting Devices Using Core-Shell (Pbs-Cds) Colloidal Quantum Dots. *Adv. Mater.* **2015**, *27*, 1437−1442.

(5) Akselrod, G. M.; Weidman, M. C.; Li, Y.; Argyropoulos, C.; Tisdale, W. A.; Mikkelsen, M. H. Efficient Nanosecond Photoluminescence from Infrared PbS Quantum Dots Coupled to Plasmonic Nanoantennas. *ACS Photonics* **2016**, *3*, 1741−1746.

(6) Hansen, M. P.; Malchow, D. S. Overview of SWIR Detectors, Cameras, and Applications. *Proc. SPIE* **2008**, *6939*, 69390I.

(7) Svensson, J.; Dey, A. W.; Jacobsson, D.; Wernersson, L.-E. III−V Nanowire Complementary Metal−Oxide Semiconductor Transistors Monolithically Integrated on Si. *Nano Lett.* **2015**, *15*, 7898−7904.

(8) Sargent, E. H. Infrared Quantum Dots. *Adv. Mater.* **2005**, *17*, 515−522.

(9) Moreels, I.; Lambert, K.; Smeets, D.; De Muynck, D.; Nollet, T.; Martins, J. C.; Vanhaecke, F.; Vantomme, A.; Delerue, C.; Allan, G.; Hens, Z. Size-Dependent Optical Properties of Colloidal PbS Quantum Dots. *ACS Nano* **2009**, *3*, 3023−3030.

(10) Kovalenko, M. V.; Manna, L.; Cabot, A.; Hens, Z.; Talapin, D. V.; Kagan, C. R.; Klimov, V. I.; Rogach, A. L.; Reiss, P.; Milliron, D. J.; Guyot-Sionnnest, P.; Konstantatos, G.; Parak, W. J.; Hyeon, T.;

(11) De Iacovo, A.; Venettacci, C.; Colace, L.; Scopa, L.; Foglia, S. High Responsivity Fire Detectors Based on PbS Colloidal Quantum Dot Photoconductors. *IEEE Photonics Technol. Lett.* **2017**, *29*, 703−706.

(12) Jin, Z.; Wang, A.; Zhou, Q.; Wang, Y.; Wang, J. Detecting Trap States in Planar PbS Colloidal Quantum Dot Solar Cells. *Sci. Rep.* **2016**, *6*, 37106.

(13) Ka, I.; Gerlein, L. F.; Asuo, I. M.; Nechache, R.; Cloutier, S. G. An Ultra-Broadband Perovskite-PbS Quantum Dot Sensitized Carbon Nanotube Photodetector. *Nanoscale* **2018**, *10*, 9044−9052.

(14) Black, A.; Roberts, J.; Acebrón, M.; Bernardo-Gavito, R.; Alsharif, G.; Urbanos, F. J.; Juárez, B. H.; Kolosov, O. V.; Robinson, B. J.; Miranda, R.; Vázquez De Parga, A. L.; Granados, D.; Young, R. J. Large-Area Heterostructures from Graphene and Encapsulated Colloidal Quantum Dots via the Langmuir-Blodgett Method. *ACS Appl. Mater. Interfaces* **2018**, *10*, 6805−6809.

(15) Maulu, A.; Rodríguez-Cantó, P. J.; Navarro-Arenas, J.; Abargues, R.; Sánchez-Royo, J. F.; García-Calzada, R.; Martínez Pastor, J. P. Strongly-Coupled PbS QD Solids by Doctor Blading for IR Photodetection. *RSC Adv.* **2016**, *6*, 80201−80212.

(16) Lambert, K.; Moreels, I.; Thourhout, D. V.; Hens, Z. Quantum Dot Micropatterning on Si. *Langmuir* **2008**, *24*, 5961−5966.

(17) Hu, C.; Aubert, T.; Justo, Y.; Flamee, S.; Cirillo, M.; Gassenq, A.; Drobchak, O.; Beunis, F.; Roelkens, G.; Hens, Z. The Micropatterning of Layers of Colloidal Quantum Dots with Inorganic Ligands Using Selective Wet Etching. *Nanotechnology* **2014**, *25*, 175302.

(18) Nandwana, V.; Subramani, C.; Yeh, Y.-C.; Yang, B.; Dickert, S.; Barnes, M. D.; Tuominen, M. T.; Rotello, V. M. Direct Patterning of Quantum Dot Nanostructures via Electron Beam Lithography. *J. Mater. Chem.* **2011**, *21*, 16859.

(19) Jagtap, A.; Goubet, N.; Livache, C.; Chu, A.; Martinez, B.; Gréboval, C.; Qu, J.; Dandeu, E.; Becerra, L.; Witkowski, N.; Ithurria, S.; Mathevet, F.; Silly, M. G.; Dubertret, B.; Lhuillier, E. Short Wave Infrared Devices Based on HgTe Nanocrystals with Air Stable Performances. *J. Phys. Chem. C* **2018**, *122*, 14979−14985.

(20) Devloo-Casier, K.; Geiregat, P.; Ludwig, K. F.; Van Stiphout, K.; Vantomme, A.; Hens, Z.; Detavernier, C.; Dendooven, J. A Case Study of ALD Encapsulation of Quantum Dots: Embedding Supported CdSe/CdS/ZnS Quantum Dots in a ZnO Matrix. *J. Phys. Chem. C* **2016**, *120*, 18039−18045.

(21) Puurunen, R. L. Surface chemistry of Atomic Layer Deposition: A Case Study for the Trimethylaluminum/Water Process. *J. Appl. Phys.* **2005**, *97*, 121301.

(22) Valdesueiro, D.; Prabhu, M. K.; Guerra-Nunez, C.; Sandeep, C. S. S.; Kinge, S.; Siebbeles, L. D. A.; De Smet, L. C. P. M.; Meesters, G. M. H.; Kreutzer, M. T.; Houtepen, A. J.; Van Ommen, J. R. Deposition Mechanism of Aluminum Oxide on Quantum Dot Films at Atmospheric Pressure and Room Temperature. *J. Phys. Chem. C* **2016**, *120*, 4266−4275.

(23) So, H.; Choi, H.; Shim, H. C.; Lee, S.; Jeong, S.; Chang, W. S. Atomic Layer Deposition Effect on the Electrical Properties of Al_2O_3-Passivated PbS Quantum Dot Field-Effect Transistors. *Appl. Phys. Lett.* **2015**, *106*, 093507.

(24) Ip, A. H.; Labelle, A. J.; Sargent, E. H. Efficient Air-Stable Colloidal Quantum Dot Solar Cells Encapsulated Using Atomic Layer Deposition of a Nanolaminate Barrier. *Appl. Phys. Lett.* **2013**, *103*, 263905.

(25) Liu, Y.; Tolentino, J.; Gibbs, M.; Ihly, R.; Perkins, C. L.; Liu, Y.; Crawford, N.; Hemminger, J. C.; Law, M. PbSe Quantum Dot Field-Effect Transistors with Air-Stable Electron Mobilities Above 7 $cm^2V^{-1}s^{-1}$. *Nano Lett.* **2013**, *13*, 1578−1587.

(26) Carlson, A.; Bowen, A. M.; Huang, Y.; Nuzzo, R. G.; Rogers, J. A. Transfer Printing Techniques for Materials Assembly and Micro/Nanodevice Fabrication. *Adv. Mater.* **2012**, *24*, 5284−5318.

(27) De Groote, A.; Cardile, P.; Subramanian, A. Z.; Fecioru, A. M.; Bower, C.; Delbeke, D.; Baets, R.; Roelkens, G. Transfer-Printing-

Based Integration of Single-Mode Waveguide-Coupled III-V-on-Silicon Broadband Light Emitters. *Laser Photon. Rev. Appl. Phys. Lett.* **2015**, *2*, 969−1004.

(28) Meitl, M. A.; Zhu, Z.-T.; Kumar, V.; Lee, K. J.; Feng, X.; Huang, Y. Y.; Adesida, I.; Nuzzo, R. G.; Rogers, J. A. Transfer Printing by Kinetic Control of Adhesion to an Elastomeric Stamp. *Nat. Mater.* **2006**, *5*, 33−38.

(29) Hendricks, M. P.; Campos, M. P.; Cleveland, G. T.; Jen-La Plante, I.; Owen, J. S. A Tunable Library of Substituted Thiourea Precursors to Metal Sulfide Nanocrystals. *Science* **2015**, *348*, 1226−30.

(30) Jung, M.-H.; Choi, H. S. Characterization of Octadecyltri-chlorosilane Self-Assembled Monolayers on Silicon (100) Surface. *Korean J. Chem. Eng.* **2009**, *26*, 1778−1784.

(31) Hsu, H.-W.; Chang, W.-C.; Tung, S.-H.; Liu, C.-L. Surface Energy-Mediated Self-Patterning for High Performance Spray-Deposited Organic Field Effect Transistors. *Adv. Mater. Interfaces* **2016**, *3*, 1500714.

(32) Konstantatos, G.; Sargent, E. H. Solution-Processed Quantum Dot Photodetectors. *Proc. IEEE* **2009**, *97*, 1666−1683.

(33) Zhang, D.; Song, J.; Zhang, J.; Wang, Y.; Zhang, S.; Miao, X. A Facile and Rapid Synthesis of Lead Sulfide Colloidal Quantum Dots Using In Situ Generated H_2S as the Sulfur Source. *CrystEngComm* **2013**, *15*, 2532.

(34) Hu, C.; Gassenq, A.; Justo, Y.; Devloo-Casier, K.; Chen, H.; Detavernier, C.; Hens, Z.; Roelkens, G. Air-Stable Short-Wave Infrared PbS Colloidal Quantum Dot Photoconductors Passivated with Al_2O_3 Atomic Layer Deposition. *Appl. Phys. Lett.* **2014**, *105*, 171110.

(35) Kim, T.-H.; Cho, K.-S.; Lee, E. K.; Lee, S. J.; Chae, J.; Kim, J. W.; Kim, D. H.; Kwon, J.-Y.; Amaratunga, G.; Lee, S. Y.; Choi, B. L.; Kuk, Y.; Kim, J. M.; Kim, K. Full-Colour Quantum Dot Displays Fabricated by Transfer Printing. *Nat. Photonics* **2011**, *5*, 176−182.

(36) Kim, T.-H.; Chung, D.-Y.; Ku, J. Y.; Song, I.; Sul, S.; Kim, D.-H.; Cho, K.-S.; Choi, B. L.; Min Kim, J.; Hwang, S.; Kim, K. Heterogeneous Stacking of Nanodot Monolayers by Dry Pick-and-Place Transfer and Its Applications in Quantum Dot Light-Emitting Diodes. *Nat. Commun.* **2013**, *4*, 2637.

(37) Kim, B. H.; Nam, S.; Oh, N.; Cho, S.-Y.; Yu, K. J.; Lee, C. H.; Zhang, J.; Deshpande, K.; Trefonas, P.; Kim, J.-H.; Lee, J.; Shin, J. H.; Yu, Y.; Lim, J. B.; Won, S. M.; Cho, Y. K.; Kim, N. H.; Seo, K. J.; Lee, H.; Kim, T.-i.; Shim, M.; Rogers, J. A. Multilayer Transfer Printing for Pixelated, Multicolor Quantum Dot Light-Emitting Diodes. *ACS Nano* **2016**, *10*, 4920−4925.

(38) De Iacovo, A.; Venettacci, C.; Colace, L.; Scopa, L.; Foglia, S. PbS Colloidal Quantum Dot Photodetectors Operating in the Near Infrared. *Sci. Rep.* **2016**, *6*, 37913.